

Fusing Global and Local: Transformer-CNN Synergy for Next-Gen Current Estimation

Junlang Huang^{1,*}, Hao Chen^{1,*}, Li Luo^{1,†}, Yong Cai^{1,†}, Lexin Zhang¹, Tianhao Ma¹, Yitian Zhang¹, Zhong Guan^{1,✉}

Abstract—This paper presents a hybrid model combining Transformer and CNN for predicting the current waveform in signal lines. Unlike traditional approaches such as current source models, driver linear representations, waveform functional fitting, or equivalent load capacitance methods, our model does not rely on fixed simplified models of standard-cell drivers or RC loads. Instead, it replaces the complex Newton iteration process used in traditional SPICE simulations, leveraging the powerful sequence modeling capabilities of the Transformer framework to directly predict current responses without iterative solving steps. The hybrid architecture effectively integrates the global feature-capturing ability of Transformers with the local feature extraction advantages of CNNs, significantly improving the accuracy of current waveform predictions.

Experimental results demonstrate that, compared to traditional SPICE simulations, the proposed algorithm achieves an error of only 0.0098. These results highlight the algorithm's superior capabilities in predicting signal line current waveforms, timing analysis, and power evaluation, making it suitable for a wide range of technology nodes, from 40nm to 3nm.

Index Terms— Signal line, RC network, current response, simulation, Transformer, CNN, Deep learning

I. INTRODUCTION

IN recent years, deep learning technologies have made remarkable progress, with Transformer-based architectures demonstrating exceptional performance and significant advantages in fields such as natural language processing (NLP), computer vision, and time-series data modeling. [1] Transformer models, by effectively capturing complex relationships and long-range dependencies, offer a novel perspective for data-driven modeling. This technological advancement has inspired researchers to explore its potential applications in traditional engineering domains, especially in complex physical modeling and signal prediction. [2]

As integrated circuit (IC) technology nodes continue to shrink, the nonlinear characteristics of standard cells and the parasitic effects of interconnects become increasingly prominent, significantly increasing the complexity of circuit simulation. The RC current response of signal lines, as a key indicator for evaluating timing, power consumption, and electromigration (EM) reliability, plays a decisive role in overall chip performance. [3] [4] To accurately analyze RC current responses and their behavior in high-speed and high-density interconnects, existing simulators typically employ traditional modeling methods. However, these methods face a trade-off between accuracy and computational efficiency, making it challenging to meet the increasingly complex demands of IC design.

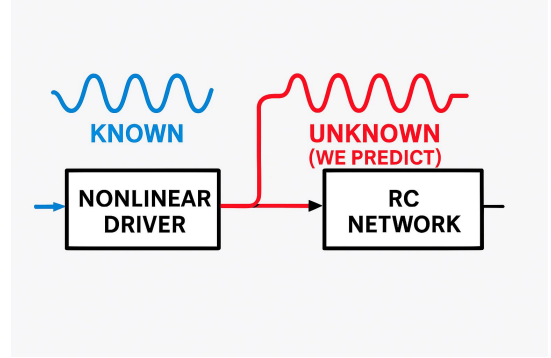


Fig. 1. **Task Description** Given a known input signal, the task is to predict the nonlinear driver's output waveform before it enters the RC network. This intermediate signal, marked in red, is unknown and serves as the prediction target of our model.

Currently, signal line RC response modeling methods can be broadly categorized into three types:

The first category is the Current Source Model (CSM). Criox and Wong proposed a gate cell current source model called Blade [5], which consists of a voltage-controlled current source, internal capacitance, and a one-step time-shift operation. Kellor further enhanced model accuracy by introducing the KTV model [6], which considers Miller capacitance. Subsequently, Li and Acar [7] and Fatemi et al. [8] introduced input and output parasitic capacitances, modeling the output current source as a function of input/output voltages, gradually incorporating nonlinear characteristics into CSM models. However, since CSM-based methods can only match fixed effective capacitances (up to two) throughout the process, the simulation accuracy of current/voltage waveforms is inherently limited [9] [10] [11] [12] [13] [14]. In recent years, widely adopted industry methods such as Composite Current Source (CCS) [15] and Extended Current Source Model (ECSM) [16] have established driver and receiver models for each cell to handle scenarios with nonlinear input and crosstalk. Nevertheless, CSM-based approaches still face significant challenges in matching high-order RC load characteristics, limiting their accuracy in current response prediction.

The second category is the Voltage Response Model (VRM), such as the Non-Linear Delay Model (NLDM). Iterative methods [17] [18] [19] [20], although capable of achieving high precision, often require substantial CPU time for convergence. Non-iterative methods [21] [22], on the other hand, rely on closed-form expressions that offer faster computation but can result in output waveform matching errors of up to 15%

[23]. Furthermore, as technology nodes shrink and RC loads become more complex, two-parameter fitting methods struggle to accurately capture the response curve of RC networks, limiting their applicability in high-precision simulations [24].

The third category consists of Direct Waveform Prediction Methods, such as double exponential functions [25], Weibull functions [26], and gamma functions [27], which directly fit the current or voltage response. Recently, a macromodeling method [28] was proposed that uses SPICE to extract parameters for modeling, which improves accuracy to some extent. However, these direct fitting methods are unable to predict initial overshoot/undershoot effects, which become more pronounced when the input slope is large.

Despite significant efforts to improve the efficiency and accuracy of predicting signal line RC responses, traditional driver-side modeling approaches often struggle to cope with the complexities of high-order RC loads. To simplify these intricate RC networks, researchers typically employ model order reduction (MOR) techniques, reducing them to effective capacitances or π -models. [29] [30] However, these methods rely on the linear characteristics of RC circuits, making it easy to overlook subtle variations and complex coupling effects within the signal lines. Consequently, achieving high precision while enhancing computational efficiency remains a critical research challenge in the field of RC response prediction.

Against this background, Transformer-based modeling methods show great potential. [1] Transformer models excel at capturing complex features and nonlinear dependencies, making them well-suited for addressing the shortcomings of traditional methods in complex signal response prediction. By incorporating Transformer models, it is possible to efficiently model signal line RC responses and leverage data-driven approaches to capture dynamic behaviors and detailed characteristics. This study aims to explore the application of Transformers in RC current response prediction, with the goal of improving simulation accuracy and computational efficiency while providing novel solutions for EM analysis and signal integrity evaluation.

This paper presents a hybrid model combining Transformer and CNN for predicting the current waveform in signal lines. Unlike traditional approaches such as current source models, driver linear representations, waveform functional fitting, or equivalent load capacitance methods, our model does not rely on fixed simplified models of standard-cell drivers or RC loads. Instead, it replaces the complex Newton iteration process used in traditional SPICE simulations, leveraging the powerful sequence modeling capabilities of the Transformer framework to directly predict current responses without iterative solving steps. The hybrid architecture effectively integrates the global feature-capturing ability of Transformers with the local feature extraction advantages of CNNs, significantly improving the accuracy of current waveform predictions.

The organization of this paper is as follows: Section II briefly introduces the theoretical background; Section III explains the data processing and the architecture of the hybrid model; Section IV compares the simulation results of classical methods with those of the proposed method; Finally, Section V provides the conclusion.

II. DATA ACQUISITION AND PREPROCESSING

A. Data Source and Simulation Configuration

1) *Simulation Environment Setup*: Simulation Environment Setup The standard cell circuit simulation environment was constructed using HSPICE, incorporating the PDK model of a 40nm CMOS technology node to ensure device parameters (e.g., threshold voltage, channel length modulation, leakage current) align with process specifications. The circuit design includes a CMOS driver unit followed by an RC signal network. The RC network parameters were generated using the SPEF (Standard Parasitic Exchange Format) netlist generator from the open-source DCTK (Digital Circuit Toolkit) platform (<https://github.com/geochrist/dctk/>), which ensures compliance with IEEE 1481-2009 standards for parasitic parameter extraction. This tool parses post-layout physical design information to generate RC networks that accurately reflect the interconnect characteristics of the target technology node.

2) *Stimulation Configuration*: Stimulation Configuration The input voltage waveform was configured as an ideal step signal (0 to VDD transition). Transient simulations covered both the signal rise/fall phases (0–10 ns) and steady-state behavior.

B. Data Preprocessing Methods

1) *Data Sources and Feature Definition*: The training data in this study is derived from HSPICE simulations, generating ground-truth results. The input features include voltage waveforms, device types, transient time, and RC parasitic parameters extracted from the SPEF netlist. The output target is the voltage response sequence. The feature definitions are as follows:

Input Features:

- **Voltage Input**: The voltage time series from transient simulation, denoted as $V(t) \in \mathbb{R}^T$, where the time step T is determined by the simulation time range.
- **Device Type**: The standard cell type, represented as categorical labels.
- **Transient Time**: The total simulation duration, denoted as $t_{\text{span}} \in \mathbb{R}^+$.
- **RC Parameters**: The extracted parasitic resistance (R) and capacitance (C) from the SPEF netlist form a two-dimensional matrix $M \in \mathbb{R}^{N \times 2}$, where N represents the number of circuit nodes.

Output Target:

- **Current Response Sequence**: The current waveform corresponding to the voltage excitation, denoted as $I(t) \in \mathbb{R}^T$.

2) *Feature Normalization*: To ensure consistency across different data modalities and improve the performance of subsequent analyses, we apply specific normalization techniques tailored to each feature type:

- **Voltage Waveform**: Dynamic range normalization is employed to scale the voltage values between 0 and 1, preserving the relative shape of the waveform:

$$V'(t) = \frac{V(t) - \min(V)}{\max(V) - \min(V)} \quad (1)$$

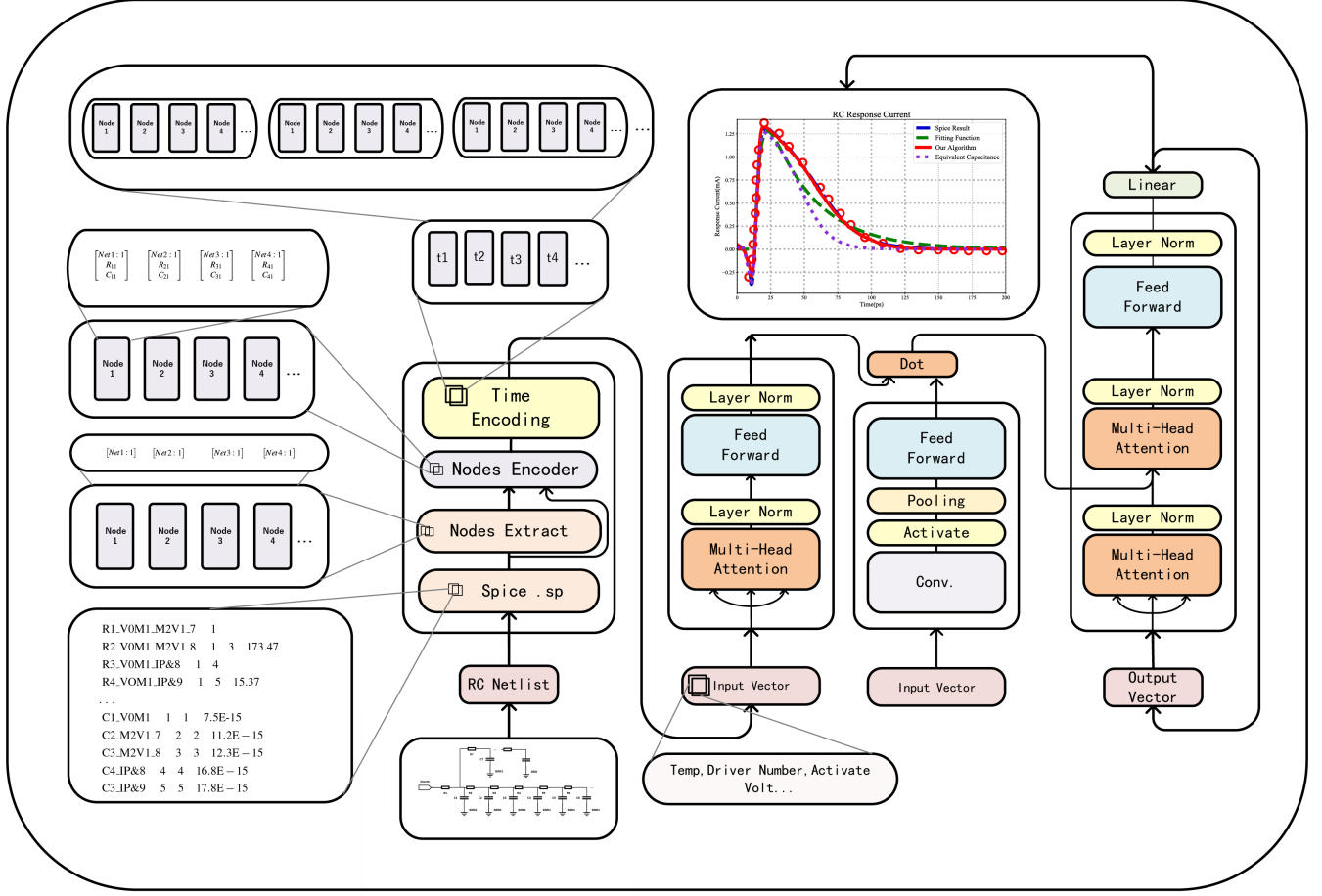


Fig. 2. **Model overview.** We extract structural features from the RC netlist using a node encoder and combine them with time encodings to form the input sequence. This input is processed in parallel by a Transformer branch for global attention and a CNN branch for local feature extraction. The outputs are fused and further refined through Transformer layers to predict the transient current response.

```
*D_NET net_0 106.518
*CONN
*I I1:Y O
*I I2:A I
*CAP
1 net_0:0 21.3035
2 net_0:1 21.3035
3 net_0:2 21.3035
4 net_0:3 21.3035
5 net_0:4 21.3035
*RES
1 I1:Y net_0:0 145.5
2 net_0:0 net_0:1 5.32588
3 net_0:1 net_0:2 5.32588
4 net_0:2 net_0:3 5.32588
5 net_0:3 net_0:4 5.32588
6 net_0:4 I2:A 145.5
*END
```

Fig. 3. An example of RC parasitic parameters in SPEF format:

Here, $V(t)$ represents the original voltage at time t , and $V'(t)$ is the normalized voltage. This transformation not only ensures that all voltage inputs are on a comparable scale but also mitigates the influence of extreme values, thereby facilitating more robust learning.

- **RC Parameters:** Z-score normalization is applied to both resistance (R) and capacitance (C) values to standardize them with a mean of 0 and a standard deviation of 1:

$$R'_i = \frac{R_i - \mu_R}{\sigma_R}, \quad C'_j = \frac{C_j - \mu_C}{\sigma_C} \quad (2)$$

In these equations, R_i and C_j are the original resistance and capacitance values, while μ_R and μ_C denote their respective means, and σ_R and σ_C their standard deviations. Standardizing RC parameters is critical to ensure that features with different scales contribute equally to the model training, thereby reducing numerical instability.

- **Transient Time:** Given the wide range of transient times, a logarithmic compression is first applied to reduce skewness, followed by Z-score normalization:

$$t'_{\text{span}} = \frac{\log_{10}(t_{\text{span}}) - \mu_t}{\sigma_t} \quad (3)$$

Here, t_{span} denotes the original transient time, and t'_{span} is the normalized value. μ_t and σ_t represent the mean and standard deviation of the log-transformed transient times. This two-step process helps in mitigating the effect of outliers and ensures that the transient time feature is well-scaled for the learning process.

Overall, these normalization steps are essential for harmonizing heterogeneous data, ensuring that each feature contributes appropriately to the model. This promotes faster convergence during training and enhances the robustness of the predictive model.

C. Detailed Procedure for SPEF Netlist Parsing and RC Parameter Flattening

This section provides a detailed explanation of the RC parameter extraction and flattening process based on SPEF netlists, covering data preprocessing, the extraction of key information, and the final mathematical representation.

1) Data Preprocessing and Key Information Definition:

According to SPEF syntax, four categories of key information are extracted for each RC element. The details are summarized in the following table:

During this process, the extracted information is appropriately normalized. For example, node positions are converted to normalized coordinates, and electrical values undergo Z-score normalization. These steps help eliminate differences in measurement scales and prepare the data for subsequent feature fusion.

D. RC Network Modeling and Feature Representation

To precisely characterize the electrical behavior of signal interconnects, we propose a graph-based fine-grained RC network modeling method. The core elements are as follows:

a) *1. Network Topology Definition:* Each signal wire is modeled as a weighted graph $\mathcal{G}_i = (\mathcal{V}_i, \mathcal{E}_i)$, where:

- The vertex set $\mathcal{V}_i = \{n_{i1}, n_{i2}, \dots, n_{iN}\}$ represents spatially discretized nodes along the wire.
- The edge set \mathcal{E}_i consists of two types of elements:
 - Resistor edges $R_{jk} \in \mathcal{E}_R$: Parasitic resistance between adjacent nodes.
 - Capacitor edges $C_{jk} \in \mathcal{E}_C$: Ground or coupling capacitance of nodes.

b) *2. Node Capacitance Modeling:* The total ground capacitance of each node n_{ij} is computed as follows:

$$C_{ij} = \underbrace{\sum_{k=1}^{M_p} c_{ijk}^{\text{para}}}_{\text{Parasitic Capacitance}} + \underbrace{\sum_{l=1}^{M_e} c_{ijl}^{\text{exp}}}_{\text{Explicit Capacitance}}$$

where M_p is the number of parasitic capacitances extracted from process data, and M_e is the number of explicit capacitors defined in the netlist.

c) *3. Effective Resistance Modeling:* Considering the impact of connection topology, a degree-weighted distribution strategy is applied:

$$R_{ij} = \sum_{k \in \mathcal{N}(j)} \frac{R_{jk}}{d_j + \epsilon}$$

where:

- $\mathcal{N}(j)$: The set of neighboring nodes of n_{ij} .
- d_j : The degree (number of connected resistors) of node j .
- ϵ : A small smoothing factor (default 10^{-6}) to avoid division by zero.

d) *4. Node Feature Encoding:* To enable batch processing by graph neural networks, each node is encoded as a 4-dimensional feature vector:

$$\mathbf{x}_{ij} = \left[\phi(i), \psi(j), \frac{C_{ij}}{C_{\text{norm}}}, \frac{R_{ij}}{R_{\text{norm}}} \right] \in \mathbb{R}^4$$

where:

- $\phi(\cdot)$: Network-level identifier extracted from the netlist, indicating which signal net the node belongs to.
- $\psi(\cdot)$: Node-level identifier extracted from the netlist, representing the node's relative position or index within the signal net.
- $C_{\text{norm}}, R_{\text{norm}}$: Normalization constants derived from training data statistics.

e) *Technical Advantages:* 1. **Physical Interpretability:** Preserves original SPEF netlist topology and device parameters. 2. **Computational Efficiency:** Degree-weighted strategy reduces $O(N^2)$ resistance mapping to $O(N)$ feature computation.

This encoding scheme effectively captures the essential physical and electrical properties of each RC element, transforming them into a unified feature vector. Such a representation is crucial for facilitating robust multi-modal feature fusion and ensuring high-quality inputs for subsequent modeling tasks.

III. HYBRID MODEL ARCHITECTURE DESIGN

A. Overall Architecture Overview

- Input: Preprocessed feature vector $X \in \mathbb{R}^{d_{in}}$ (dimension $d_{in} = N_{time} + N_{RC} + N_{device}$)
- Output: Predicted voltage waveform sequence $Y \in \mathbb{R}^T$ (time steps T determined by transient time)

This model adopts a hybrid architecture. After being uniformly encoded by the embedding layer, the input is fed in parallel into a CNN branch and a three-layer Transformer encoder (multi-head attention to model global voltage temporal dependencies). The fused features obtained through concatenation are then passed into a three-layer Transformer decoder (masked self-attention and cross-modal attention). Finally, the predicted voltage waveform is generated through a fully connected layer.

B. Input Embedding Layer

Function: Map heterogeneous features to a unified latent space.

- **Fully Connected (FC) Projection:** [31]

$$H_0 = \text{ReLU}(W_e X + b_e), \quad W_e \in \mathbb{R}^{d_{\text{embed}} \times d_{\text{in}}} \quad (4)$$

- **Output Dimension:**

$$H_0 \in \mathbb{R}^{L \times d_{\text{embed}}} \quad (5)$$

(L represents the sequence length, extended by time steps.)

C. CNN Architecture Design

1) *Input Feature Adaptation:* The input to the CNN branch is the time-series feature tensor output from the embedding layer $\mathbf{X}_{\text{embed}} \in \mathbb{R}^{B \times L \times D}$, where B is the batch size, L is the sequence length, and D is the embedding dimension. To adapt to the 1D convolution operation, the input tensor is dimensionally rearranged as follows:

$$\mathbf{X}_{\text{reshape}} = \text{Permute}(\mathbf{X}_{\text{embed}}) \in \mathbb{R}^{B \times D \times L} \quad (6)$$

This operation transforms the embedding dimension D into the channel dimension, matching the convolutional layer input format (B, C, L) .

2) *Convolutional Feature Extraction:* [32] A single-layer 1D convolution kernel is employed to capture local temporal patterns, mathematically expressed as:

$$\mathbf{H}_{\text{conv}} = \text{ReLU}(\mathbf{X}_{\text{reshape}} * \mathbf{W}_{\text{conv}} + \mathbf{b}_{\text{conv}}) \in \mathbb{R}^{B \times K \times L'} \quad (7)$$

Here, $*$ denotes the convolution operation, $\mathbf{W}_{\text{conv}} \in \mathbb{R}^{K \times D \times S}$ represents the learnable weights (K is the number of output channels, S is the kernel size), and:

$$L' = \left\lfloor \frac{(L - S)}{1} + 1 \right\rfloor \quad (8)$$

is the post-convolution sequence length.

3) *Feature Space Mapping:* Feature compression and dimensionality restoration are achieved through two fully connected layers:

$$\mathbf{H}_{\text{dense1}} = \text{ReLU}(\mathbf{W}_1 \mathbf{H}_{\text{conv}} + \mathbf{b}_1) \in \mathbb{R}^{B \times K \times M} \quad (9)$$

$$\mathbf{H}_{\text{out}} = \mathbf{W}_2 \mathbf{H}_{\text{dense1}} + \mathbf{b}_2 \in \mathbb{R}^{B \times D \times L'} \quad (10)$$

Here, M is the intermediate hidden layer dimension, $\mathbf{W}_1 \in \mathbb{R}^{M \times K}$ and $\mathbf{W}_2 \in \mathbb{R}^{D \times M}$ are learnable weight matrices. The final output is dimensionally restored to align with the Transformer branch:

$$\mathbf{X}_{\text{cnn}} = \text{Permute}(\mathbf{H}_{\text{out}}) \in \mathbb{R}^{B \times L' \times D} \quad (11)$$

The CNN module captures local patterns in the input sequence through convolution operations and transforms the feature space via fully connected layers, thereby capturing the correlations of the local RC network topology and enhancing the recognition of RC network information. Specifically, the

local receptive field is constrained by using a convolution kernel of size $S = 3$ [33], which limits the extraction range and forces the model to focus on the RC topological relationships of neighboring time steps. Feature interaction is lightweight as the dimensionality reduction is performed using fully connected layers rather than pooling, preserving the complete temporal resolution. Additionally, the final output dimension D is maintained equal to the input embedding dimension, ensuring compatibility for multimodal feature fusion.

D. Encoder Architecture and Feature Fusion Strategy

The Transformer encoder layer comprises a **multi-head self-attention mechanism** and a **feedforward neural network** [1], both integrated with residual connections and layer normalization to facilitate deep feature learning. The mathematical formulation is as follows:

1) *Input Feature Preprocessing:* Let the input tensor be defined as $X \in \mathbb{R}^{B \times L \times D}$, where B denotes the batch size, L represents the sequence length, and D corresponds to the embedding dimension. The encoder directly receives inputs either from the embedding layer or from the output of a preceding encoder layer.

2) *Multi-Head Self-Attention Mechanism:* Self-attention is first computed by transforming the input through learnable parameter matrices $W_Q, W_K, W_V \in \mathbb{R}^{D \times D}$ to generate the Query (Q), Key (K), and Value (V) matrices [1]:

$$Q = XW_Q, \quad K = XW_K, \quad V = XW_V \quad (12)$$

The input is then split into h attention heads, and each head computes scaled dot-product attention independently:

$$\text{head}_i = \text{Softmax} \left(\frac{Q_i K_i^T}{\sqrt{D/h}} \right) V_i \quad (13)$$

The outputs from all attention heads are concatenated and projected as follows:

$$\text{MHA}(X) = \text{Concat}(\text{head}_1, \dots, \text{head}_h) W_O \quad (14)$$

where $W_O \in \mathbb{R}^{D \times D}$ is the output projection matrix.

3) *Residual Connection and Layer Normalization:* To ensure stable gradient propagation and enhance training stability, a residual connection is applied, followed by layer normalization [34] [35]:

$$X' = \text{LayerNorm}(X + \text{Dropout}(\text{MHA}(X))) \quad (15)$$

This serves two key purposes:

- **Residual Connection:** Helps mitigate gradient vanishing while preserving original feature representations [36].
- **Layer Normalization:** Improves training stability and accelerates convergence by normalizing activations across feature dimensions.

4) *Feedforward Neural Network:* A position-wise feedforward network further enhances the model's expressive power by applying two linear transformations interleaved with a non-linear activation function:

$$F = W_2 \cdot \text{ReLU}(W_1 X' + b_1) + b_2 \quad (16)$$

where $W_1 \in \mathbb{R}^{D \times d_{ff}}$, $W_2 \in \mathbb{R}^{d_{ff} \times D}$, and d_{ff} denotes the dimensionality of the hidden layer.

5) *Second Residual Connection and Normalization*: A second residual connection and layer normalization are then applied to refine the learned representations [37]:

$$X'' = \text{LayerNorm}(X' + \text{Dropout}(F)) \quad (17)$$

6) *Encoder Output*: The final output tensor $X'' \in \mathbb{R}^{B \times L \times D}$ is passed either to the subsequent encoder layer or to the decoder for further processing.

7) *Feature Fusion via Dot Product*: To effectively integrate global representations from the Transformer encoder and local features extracted by the CNN, we perform an element-wise dot product operation [1]:

$$H_{\text{fusion}} = X'' \odot X_{\text{cnn}} \quad (18)$$

where $X'' \in \mathbb{R}^{B \times L \times D}$ is the output from the Transformer encoder, $X_{\text{cnn}} \in \mathbb{R}^{B \times L \times D}$ is the output from the CNN branch, and \odot denotes element-wise multiplication. This fusion mechanism enhances the interaction between sequential and spatial dependencies.

8) *Decoder Input Projection*: To ensure compatibility with the decoder input format, we apply a linear projection:

$$H_{\text{decoder}} = W_f H_{\text{fusion}} + b_f, \quad H_{\text{decoder}} \in \mathbb{R}^{B \times L \times D} \quad (19)$$

where $W_f \in \mathbb{R}^{D \times D}$ and $b_f \in \mathbb{R}^D$ are trainable parameters. The transformed feature representation H_{decoder} is then fed into the Transformer decoder for further processing.

E. Transformer Decoder Architecture

The Transformer decoder is responsible for generating the target sequence by leveraging masked self-attention and encoder-decoder cross-attention mechanisms. The mathematical formulation is outlined as follows.

1) *Input Definition*: Let the decoder input be defined as

$$Y \in \mathbb{R}^{B \times T \times D}, \quad (20)$$

which represents the target sequence embeddings, and let the encoder output be

$$H_{\text{enc}} \in \mathbb{R}^{B \times L \times D}, \quad (21)$$

where T denotes the target sequence length, L represents the source sequence length, and B and D indicate the batch size and embedding dimension, respectively.

2) *Masked Multi-Head Self-Attention*: [1]

Causal Masking: To prevent information leakage from future time steps, a lower triangular mask is applied to the self-attention score matrix:

$$\text{Mask}_{ij} = \begin{cases} 0, & i \geq j, \\ -\infty, & i < j. \end{cases} \quad (22)$$

Attention Calculation: The masked self-attention mechanism is computed as follows:

$$\text{Attn}_{\text{self}} = \text{Softmax}\left(\frac{QK^T}{\sqrt{D}} + \text{Mask}\right)V, \quad (23)$$

where

$$Q = K = V = YW_{QKV}, \quad (24)$$

with $W_{QKV} \in \mathbb{R}^{D \times D}$ being a learnable projection matrix. This mechanism ensures that each position in the target sequence can only attend to previous positions, preserving the autoregressive nature of decoding.

3) *Encoder-Decoder Cross-Attention*: **Cross-Modal Interaction**: The encoder-decoder cross-attention mechanism enables the decoder to incorporate contextual information from the encoder output. Specifically, the intermediate decoder representation is used as the query, while the encoder output serves as the key-value pair:

$$\text{Attn}_{\text{cross}} = \text{Softmax}\left(\frac{Q_{\text{dec}}K_{\text{enc}}^T}{\sqrt{D}}\right)V_{\text{enc}}, \quad (25)$$

where

$$Q_{\text{dec}} = Y'W_Q, \quad (26)$$

with Y' representing the processed decoder input and $W_Q \in \mathbb{R}^{D \times D}$ being a trainable projection matrix. This mechanism aligns the target sequence generation with the source sequence representations, facilitating effective sequence-to-sequence modeling.

4) *Feedforward Neural Network*: To enhance feature representations, a two-layer feedforward network is applied:

$$F = W_2 \cdot \text{GELU}(W_1 Y'' + b_1) + b_2, \quad (27)$$

where $W_1 \in \mathbb{R}^{D \times d_{ff}}$, $W_2 \in \mathbb{R}^{d_{ff} \times D}$, $b_1 \in \mathbb{R}^{d_{ff}}$, and $b_2 \in \mathbb{R}^D$. Here, d_{ff} denotes the hidden layer dimension of the feedforward network. The GELU activation function is employed to introduce non-linearity and improve gradient flow during training [38].

5) *Summary*: In summary, the decoder architecture sequentially applies masked self-attention to model intra-target dependencies, encoder-decoder cross-attention to incorporate contextual representations from the encoder, and a feedforward network to refine the learned representations. This hierarchical structure ensures effective target sequence generation while preserving temporal causality.

IV. RESULTS

A. Scalability Across Network Sizes

To evaluate the scalability of our neural network model with respect to increasing circuit complexity, we constructed a set of networks with varying numbers of RC nets, ranging from 2 to 100. For each network configuration, we simulated the voltage response using both our neural network predictor and a SPICE-based transient solver.

The results, shown in Table I, indicate that the RMSE generally decreases as n increases from 2 to 80, suggesting that the ensemble of more sub-networks enhances the model's representation capability. The best performance was achieved at $n = 80$ with an RMSE of **0.0020**, followed closely by $n = 70$ and $n = 90$. However, when n increased to 100, the RMSE sharply rose to **0.0098**, indicating possible overfitting or optimization instability. These findings demonstrate that while increasing n generally improves performance, there exists an optimal range ($n \in [70, 90]$) beyond which the model may degrade.

TABLE I
VALIDATION RMSE FOR DIFFERENT NUMBERS OF SUBNETWORKS n ON THE RC_1 DATASET.

Number of Networks (n)	Validation RMSE
2	0.0079
5	0.0043
10	0.0074
15	0.0045
20	0.0029
30	0.0042
40	0.0057
50	0.0032
60	0.0067
70	0.0021
80	0.0020
90	0.0023
100	0.0098

Figure below shows the root mean squared error (RMSE) between the predicted and ground-truth voltage waveforms as a function of the network size. Notably, the prediction accuracy remains consistent even as the number of internal nodes increases, with only a modest rise in error for the largest networks. This demonstrates that the model can generalize well to large-scale RC networks, indicating its potential for hierarchical or full-chip level timing analysis.

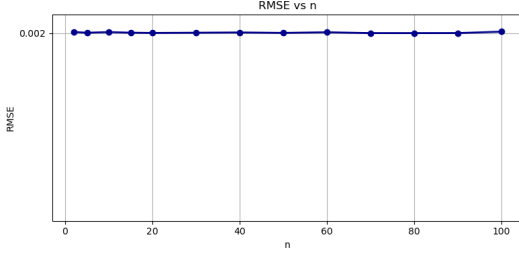


Fig. 4. rmse_vs_n

B. Accuracy of Voltage Response Prediction

We further quantified the accuracy of our model by comparing its output against SPICE simulations across a wide range of RC networks with diverse topologies and parameter settings. The comparison was performed on a held-out test set of 100 RC configurations not seen during training.

Figure 5 shows an example voltage trace comparison between the SPICE ground truth and the neural network prediction for a representative circuit. The predicted waveform (orange dashed line) closely matches the true response (blue solid line), accurately capturing the rise behavior, steady-state voltage level, and response curvature. Notably, the model predicts the early-stage transient response with high fidelity, which is critical in timing-sensitive applications.

Across the full test set, the RMSE was measured at 0.009813355. These results confirm that the proposed model achieves high-fidelity predictions, rivaling traditional circuit simulators in accuracy while significantly reducing inference time.

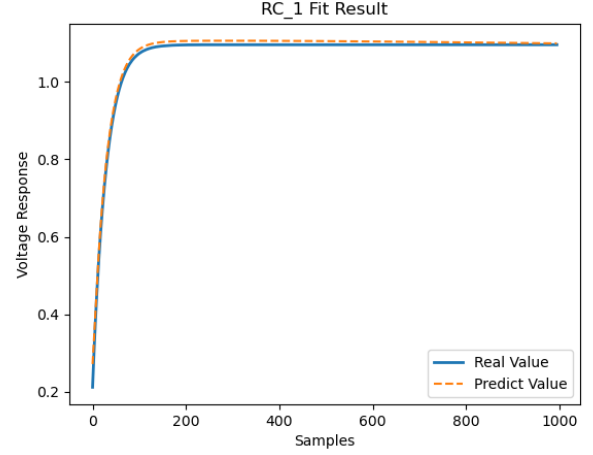


Fig. 5. Comparison of voltage response between SPICE simulation and neural network prediction on a representative RC network.

C. Training time and Infer time Comparison

As shown in Table II, the training time remains relatively stable across different numbers of sub-networks n , ranging from approximately 77 to 80 seconds. This indicates that the increase in model capacity due to higher n values does not significantly impact the training runtime, likely due to efficient batching and parallelization during training.

TABLE II
TRAINING TIME (IN SECONDS) FOR DIFFERENT NUMBER OF SUB-NETWORKS n .

Number of Networks (n)	Training Time (s)
2	78.19
5	79.25
10	77.53
15	79.39
20	77.59
30	77.69
40	77.93
50	78.24
60	78.89
70	78.44
80	78.64
90	80.43
100	79.54

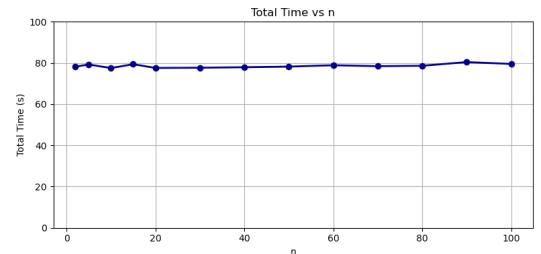


Fig. 6. Total_Time_vs_n

V. FUTURE CHALLENGES AND DIRECTIONS FOR OUR MODEL

VI. FUTURE CHALLENGES AND DIRECTIONS

Despite the promising results achieved by our neural predictor, several challenges remain before it can be adopted in broader circuit analysis workflows. In this section, we discuss key limitations of the current approach and highlight potential directions for future research.

A. Limited Generalization Across Topologies

One of the main limitations of the current model is its restricted ability to generalize across circuits with different topological complexities. The model is trained on RC networks with fixed-size inputs and relatively homogeneous structure, which limits its applicability to networks with varied node counts, branch configurations, or dynamic component distributions. When applied to a topology unseen during training, the prediction accuracy tends to degrade significantly. Addressing this challenge requires the development of topology-aware or topology-invariant architectures. For instance, graph-based neural networks (GNNs) that operate directly on circuit graphs could offer a more flexible representation, enabling better generalization across a wider variety of network configurations.

B. Quadratic Complexity of Transformer Inference

The current architecture relies on the standard Transformer encoder-decoder framework, which incurs quadratic computational complexity $\mathcal{O}(n^2)$ with respect to the input sequence length n due to the self-attention mechanism. Although this cost is manageable for small circuits, it becomes prohibitive for larger-scale networks with hundreds or thousands of nodes. Reducing this bottleneck is essential for scaling to industrial-grade circuit sizes. Recent advances in efficient Transformers, such as Linformer, Performer, or Longformer, which reduce attention complexity to linear or sub-quadratic time, present viable alternatives that could be integrated into future versions of the model.

C. Temporal Alignment and Stability Under Noise

Another challenge lies in ensuring the temporal alignment of predicted and true voltage waveforms, especially in high-frequency transients. While the model performs well under nominal conditions, it may exhibit phase drift or temporal misalignment when circuit parameters vary significantly or when input signals are noisy. This suggests the need for explicit mechanisms to model temporal causality and uncertainty. Incorporating recurrent components (e.g., gated RNNs) or probabilistic modeling (e.g., Bayesian neural nets) could enhance the model's robustness to such variations.

D. Lack of Physical Interpretability and Control

Finally, like many black-box neural models, the current predictor lacks interpretability and offers limited control over specific electrical behaviors (e.g., delay tuning, overshoot

suppression). This poses challenges for deployment in design-in-the-loop settings where precise control is required. Future work may consider embedding circuit-theoretic constraints or physical priors directly into the model architecture or training loss. Hybrid models that combine learnable components with analytical solvers could strike a balance between accuracy, efficiency, and interpretability.

In summary, while our work demonstrates that neural networks can serve as fast and accurate circuit response predictors, substantial efforts are still needed to bridge the gap toward general-purpose, scalable, and controllable neural circuit solvers. We leave these directions for future exploration.

VII. CONCLUSION

In this work, we presented an initial demonstration of a neural network-based surrogate model for fast prediction of voltage responses in RC networks. The proposed architecture integrates Transformer encoders and convolutional modules to simultaneously capture temporal dependencies and spatial features across network nodes. By leveraging structured input representations of circuit topology and component values, the model is able to learn complex transient behaviors with high accuracy.

Through experiments on synthetic RC networks with varying parameters, we showed that the model can closely approximate the voltage trajectories obtained from SPICE simulations, while significantly reducing inference time. Our results confirm the feasibility of applying deep learning to analog circuit modeling tasks, and highlight the potential of hybrid architectures in capturing both global context and local signal dynamics.

This first-stage demonstration provides a foundation for future extensions toward more generalized, scalable, and interpretable neural solvers. In subsequent work, we aim to further enhance the model's adaptability to diverse topologies and explore integration with traditional simulation frameworks.

REFERENCES

- [1] A. Vaswani, N. Shazeer, N. Parmar, J. Uszkoreit, L. Jones, A. N. Gomez, E. Kaiser, and I. Polosukhin, "Attention is all you need," *Advances in neural information processing systems*, vol. 30, 2017.
- [2] J. Devlin, M.-W. Chang, K. Lee, and K. Toutanova, "Bert: Pre-training of deep bidirectional transformers for language understanding," in *Proceedings of the 2019 conference of the North American chapter of the association for computational linguistics: human language technologies, volume 1 (long and short papers)*, pp. 4171–4186, 2019.
- [3] J. R. Black, "Electromigration—a brief survey and some recent results," *IEEE Transactions on Electron Devices*, vol. 16, no. 4, pp. 338–347, 1969.
- [4] D. K. Sharma, B. Kaushik, and R. Sharma, "Vlsi interconnects and their testing: prospects and challenges ahead," *Journal of Engineering, Design and Technology*, vol. 9, no. 1, pp. 63–84, 2011.
- [5] J. F. Croix and D. Wong, "Blade and razor: cell and interconnect delay analysis using current-based models," in *Proceedings of the 40th annual Design Automation Conference*, pp. 386–389, 2003.
- [6] I. Keller, K. Tseng, and N. Verghese, "A robust cell-level crosstalk delay change analysis," in *IEEE/ACM International Conference on Computer Aided Design, 2004. ICCAD-2004.*, pp. 147–154, IEEE, 2004.
- [7] P. Li and E. Acar, "A waveform independent gate model for accurate timing analysis," in *2005 International Conference on Computer Design*, pp. 363–365, IEEE, 2005.

- [8] H. Fatemi, S. Nazarian, and M. Pedram, "Statistical logic cell delay analysis using a current-based model," in *Proceedings of the 43rd annual Design Automation Conference*, pp. 253–256, 2006.
- [9] C. Amin, C. Kashyap, N. Menezes, K. Killpack, and E. Chiprout, "A multi-port current source model for multiple-input switching effects in cmos library cells," in *Proceedings of the 43rd annual Design Automation Conference*, pp. 247–252, 2006.
- [10] C. Kashyap, C. Amin, N. Menezes, and E. Chiprout, "A nonlinear cell macromodel for digital applications," in *2007 IEEE/ACM International Conference on Computer-Aided Design*, pp. 678–685, IEEE, 2007.
- [11] N. Menezes, C. Kashyap, and C. Amin, "A true electrical cell model for timing, noise, and power grid verification," in *Proceedings of the 45th annual Design Automation Conference*, pp. 462–467, 2008.
- [12] B. Amelifard, S. Hatami, H. Fatemi, and M. Pedram, "A current source model for cmos logic cells considering multiple input switching and stack effect," in *Proceedings of the conference on Design, automation and test in Europe*, pp. 568–573, 2008.
- [13] S. Nazarian, H. Fatemi, and M. Pedram, "Accurate timing and noise analysis of combinational and sequential logic cells using current source modeling," *IEEE transactions on very large scale integration (VLSI) systems*, vol. 19, no. 1, pp. 92–103, 2010.
- [14] N. K. Katam and M. Pedram, "Timing characterization for static timing analysis of single flux quantum circuits," *IEEE Transactions on Applied Superconductivity*, vol. 29, no. 6, pp. 1–8, 2019.
- [15] Synopsys, "Composite current source (ccs)." Online. Accessed: 2025-03-29.
- [16] C. D. Systems, "Effective current source model (ecsm)." Online. Accessed: 2025-03-29.
- [17] J. Qian, S. Pullela, and L. Pillage, "Modeling the effective capacitance for the rc interconnect of cmos gates," *IEEE Transactions on Computer-Aided Design of Integrated Circuits and Systems*, vol. 13, no. 12, pp. 1526–1535, 1994.
- [18] S. Abbaspour and M. Pedram, "Calculating the effective capacitance for the rc interconnect in vdsmt technologies," in *Proceedings of the 2003 Asia and South Pacific Design Automation Conference*, pp. 43–48, 2003.
- [19] F. Dartu, N. Menezes, and L. T. Pileggi, "Performance computation for precharacterized cmos gates with rc loads," *IEEE Transactions on Computer-Aided Design of Integrated Circuits and Systems*, vol. 15, no. 5, pp. 544–553, 1996.
- [20] J. M. Wang, J. Li, S. Yanamanamanda, L. K. Vakati, and K. K. Muchherla, "Modeling the driver load in the presence of process variations," *IEEE Transactions on Computer-Aided Design of Integrated Circuits and Systems*, vol. 25, no. 10, pp. 2264–2275, 2006.
- [21] A. B. Kahng and S. Muddu, "Improved effective capacitance computations for use in logic and layout optimization," in *Proceedings Twelfth International Conference on VLSI Design.(Cat. No. PR00013)*, pp. 578–582, IEEE, 1999.
- [22] M. Shao, M. D. Wong, H. Cao, Y. Gao, L.-P. Yuan, L.-D. Huang, and S. Lee, "Explicit gate delay model for timing evaluation," in *Proceedings of the 2003 international symposium on Physical design*, pp. 32–38, 2003.
- [23] M. Jiang, Q. Li, Z. Huang, and Y. Inoue, "A non-iterative effective capacitance model for cmos gate delay computing," in *2010 International Conference on Communications, Circuits and Systems (ICCCAS)*, pp. 896–900, IEEE, 2010.
- [24] D. Garyfallou, S. Simoglou, N. Sketopoulos, C. Antoniadis, C. P. Sotiriou, N. Evmorfopoulos, and G. Stamoulis, "Gate delay estimation with library compatible current source models and effective capacitance," *IEEE Transactions on Very Large Scale Integration (VLSI) Systems*, vol. 29, no. 5, pp. 962–972, 2021.
- [25] P. Jain and A. Jain, "Accurate current estimation for interconnect reliability analysis," *IEEE Transactions on very large scale Integration (VLSI) Systems*, vol. 20, no. 9, pp. 1634–1644, 2011.
- [26] C. S. Amin, F. Dartu, and Y. I. Ismail, "Weibull-based analytical waveform model," *IEEE Transactions on Computer-Aided Design of Integrated Circuits and Systems*, vol. 24, no. 8, pp. 1156–1168, 2005.
- [27] T. Lin, E. Acar, and L. Pileggi, "h-gamma: an rc delay metric based on a gamma distribution approximation of the homogeneous response," in *Proceedings of the 1998 IEEE/ACM international conference on Computer-aided design*, pp. 19–25, 1998.
- [28] N. Mirzaie and R. Rohrer, "A macromodeling approach for analog behavior of digital integrated circuits," *IEEE Transactions on Computer-Aided Design of Integrated Circuits and Systems*, vol. 39, no. 12, pp. 5025–5031, 2020.
- [29] A. Odabasioglu, M. Celik, and L. T. Pileggi, *PRIMA: Passive reduced-order interconnect macromodeling algorithm*. Springer, 2003.
- [30] K. Cheng, Z. Ye, and W. Yu, "Model order reduction for large scale rc networks based on optimal elimination," *Journal of Computer-Aided Design & Computer Graphics*, vol. 24, no. 11, pp. 1506–1512, 2012.
- [31] Y. Bengio, R. Ducharme, P. Vincent, and C. Jauvin, "A neural probabilistic language model," *Journal of machine learning research*, 2003.
- [32] S. Bai, J. Z. Kolter, and V. Koltun, "An empirical evaluation of generic convolutional and recurrent networks for sequence modeling," *arXiv preprint arXiv:1803.01271*, 2018.
- [33] Y. Lecun, L. Bottou, Y. Bengio, and P. Haffner, "Gradient-based learning applied to document recognition," *Proceedings of the IEEE*, 1998.
- [34] J. L. Ba, J. R. Kiros, and G. E. Hinton, "Layer normalization," *arXiv preprint arXiv:1607.06450*, 2016.
- [35] N. Srivastava, G. Hinton, A. Krizhevsky, I. Sutskever, and R. Salakhutdinov, "Dropout: A simple way to prevent neural networks from overfitting," *The journal of machine learning research*, vol. 15, no. 1, pp. 1929–1958, 2014.
- [36] K. He, X. Zhang, S. Ren, and J. Sun, "Deep residual learning for image recognition," in *Proceedings of the IEEE conference on computer vision and pattern recognition*, 2016.
- [37] R. Xiong, Y. Yang, D. He, K. Zheng, S. Zheng, C. Xing, H. Zhang, Y. Lan, L. Wang, and T. Liu, "On layer normalization in the transformer architecture," in *International conference on machine learning*, pp. 10524–10533, PMLR, 2020.
- [38] D. Hendrycks and K. Gimpel, "Gaussian error linear units (gelus)," *arXiv preprint arXiv:1606.08415*, 2016.